UNICAMP

IFGW
Instituto de Física Gleb Wataghin
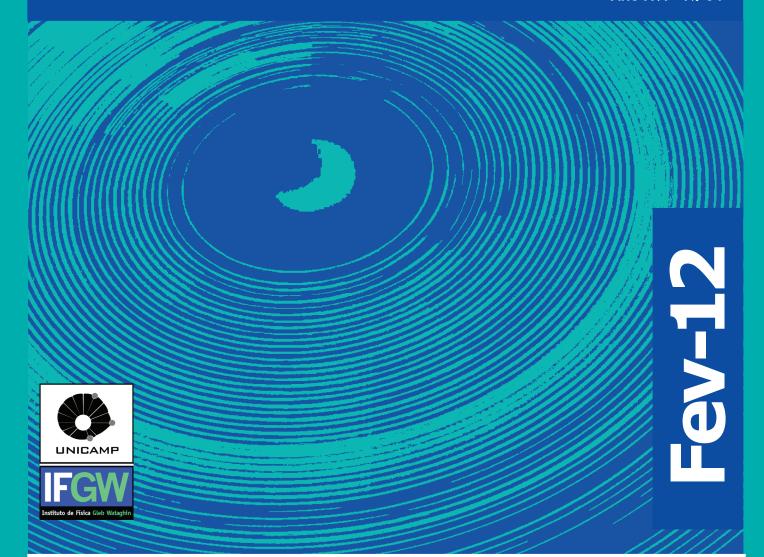
Trabalhos Publicados

Dezembro 2011 à Fevereiro 2012

P001-12 à P038-12

Material Editorial

Trabalhos Publicados

[P001-12] "Anisotropic Growth of Water-Puckered Pentamers on a Mica Terrace"

Teschke, O., Bonugli, L. O., de Souza, E. F.

Ice nucleation at mica terrace edges in air forms mounds of water molecules that grow larger as the step-edge height increases from a few Angstroms to hundreds of nanometers. The structures of the ice deposits at mica terrace edges were characterized by atomic force microscopy (AFM), and the edges were shown to act as nucleators for water pentamers, thereby forming a zigzag structure with lattice parameters of 0.72 +/- 0.07 and 0.60 +/- 0.06 nm. A three-dimensional arrangement of three pentamers of water molecules, which formed a parasol-like structure, was assembled to match the AFM images. Seven three-fused pentamers were clustered to form large hexamers that cover the entire surface. The nucleation at the edges reveals a substantially larger growth rate than that on the mica terraces; consequently, highly terraced mica slabs could be used as new and more efficient structures for seeding clouds and causing rain. On the basis of this finding, a new ice-condensation structure was designed with pyramidal features and steps of 100 nm in height and width.

[P002-12] "Black holes surrounded by thin rings and the stability of circular orbits"

de Castro, G. M., Letelier, P. S.

The solution to the Einstein vacuum field equation associated with a nonlinear superposition of a Kerr black hole with a thin ring of constant density is studied. The method used is the vesture method of Belinsky and Zakharov. The Newtonian ring potential is approximated by a truncate multipolar expansion. This expansion is used as a seed solution in the above-mentioned method. Estimations of errors due to the truncation of the multipolar expansions are performed. The epicyclic and vertical stabilities of circular equatorial orbits related to particles moving around the system black hole surrounded by a ring are considered for both relativistic and Newtonian gravity. We find the unexpected effect of the duplication of the photon circular orbit for certain values of the parameters related to the black hole and ring.

[P003-12] "Carbon support treatment effect on Ru/C catalyst performance for benzene partial hydrogenation"

Zanutelo, C., Landers, R., Carvalho, W. A., Cobo, A. J. G.

Ru/C catalysts were prepared from commercial activated carbon submitted to different treatments. The catalysts were prepared by incipient wetness impregnation, through an aqueous solution of the precursor $RuCl_3 \cdot xH_2O$. After impregnation, some catalysts were submitted to direct reduction treatment under H_2 flow at the temperature of 150 degrees C, in order to evaluate the effects of activation. The supports were characterized by N_2 adsorption, Boehm and potentiometric titration. The X-ray photoelectron spectroscopy was used to study the supports and catalysts surfaces, while scanning electron microscopy allowed us to determine the chemical composition and observe the catalysts morphology. Ru/C catalysts performance was evaluated within the hydrogenation reaction of benzene in liquid phase, using a Parr reactor. The reaction was conducted under total pressure of 5.0 MPa of H_2, at a temperature of 100 degrees C with water in the reaction medium. The obtained results indicate that the Ru/C system catalytic performance is influenced for determined functional groups present on the activated carbon surface.

The carbonyl groups decrease the activity and selectivity of the reactions, while an increase of the carboxylic groups leads to more active catalysts and the highest yield of cyclohexene.

[P004-12] "CdTe and CdSe Quantum Dots Cytotoxicity: A Comparative Study on Microorganisms"

Gomes, S. A. O., Vieira, C. S., Almeida, D. B., Santos-Mallet, J. R., Menna-Barreto, R. F. S., Cesar, C. L., Feder, D.

Quantum dots (QDs) are colloidal semiconductor nanocrystals of a few nanometers in diameter, being their size and shape controlled during the synthesis. They are synthesized from atoms of group II-VI or III-V of the periodic table, such as cadmium telluride (CdTe) or cadmium selenium (CdSe) forming nanoparticles with fluorescent characteristics superior to current fluorophores. The excellent optical characteristics of quantum dots make them applied widely in the field of life sciences. Cellular uptake of QDs, location and translocation as well as any biological consequence, such as cytotoxicity, stimulated a lot of scientific research in this area. Several studies pointed to the cytotoxic effect against micoorganisms. In this mini-review, we overviewed the synthesis and optical properties of QDs, and its advantages and bioapplications in the studies about microorganisms such as protozoa, bacteria, fungi and virus.

[P005-12] "Comparative parametric method 6 (PM6) and Recife model 1 (RM1) study of trans-stilbene"

Camilo, A., dos Santos, R. P. B., Coluci, V. R., Galvao, D. S.

In this paper, we report a comparative parametric method 6 (PM6) and Recife model 1 (RM1) study of trans-stilbene in its ground and (excited) singlet, triplet and ionic (positive and negative polarons and bipolarons) states. We evaluated the accuracy of the recently developed PM6 and RM1 comparing the obtained results with other semi-empirical, ab initio methods and available experimental data. PM6 and RM1 predict non-planar ground and singlet states for trans-stilbene, in agreement with the PM5 and the Austin model 1. On the other hand, the PM3 predicts planar configurations, which is in agreement with the available experimental data. PM6 and RM1 overestimate the cis-trans isomerisation energy as well as the ionisation potential of both cis-and trans-stilbene. In spite of the developments of these new methods, PM3 continues to be the only one of these methods to correctly predict the conformation of stilbene.

[P006-12] "Complex mixed state of the Pauli-limited superconductor CeCoIn5"

Gratens, X., Mendonca-Ferreira, L., Kopelevich, Y., Oliveira, N. F., Urbano, R. R., Ribeiro, R. A., Movshovich, R., Sarrao, J. L., Thompson, J. D., Fisk, Z., Pagliuso, P. G.

Magnetization measurements were performed on CeCoIn5 at temperatures down to 20 mK and magnetic fields up to 17 T applied along different crystallographic orientations. For field configurations nearly parallel to the ab plane (theta less than or similar to 40 degrees and T <= 50 mK), we have found an intriguing vortex dynamics regime revealed by a hysteretic and metastable anomalous peak effect (APE), which gives evidence of surface barrier effects enhanced by antiferromagnetic fluctuations in the mixed state of CeCoIn5. Furthermore,

we have observed crossover features in the torque and magnetization traces at fields below H-c2, which are consistent with vortices lattice phase transitions and with the anomalies speculated to be the Fulde-Ferrel-Larkin-Ovchinnikov (FFLO) superconducting state in CeCoIn5. All of the above features were found to be dramatically perturbed in Ce0.98Gd0.02CoIn5.

[P007-12] "Co-Substitution Effects on the Fe Valence in the BaFe(2)As(2) Superconducting Compound: A Study of Hard X-Ray Absorption Spectroscopy"

Bittar, E. M., Adriano, C., Garitezi, T. M., Rosa, P. F. S., Mendonca-Ferreira, L., Garcia, F., Azevedo, G. D., Pagliuso, P. G., Granado, E.

The Fe K x-ray absorption near edge structure of BaFe(2-x)Co(x)As(2) superconductors was investigated. No appreciable alteration in shape or energy position of this edge was observed with Co substitution. This result provides experimental support to previous ab initio calculations in which the extra Co electron is concentrated at the substitute site and do not change the electronic occupation of the Fe ions. Superconductivity may emerge due to bonding modifications induced by the substitute atom that weakens the spin-density-wave ground state by reducing the Fe local moments and/or increasing the elastic energy penalty of the accompanying orthorhombic distortion.

[P008-12] "Detection of point sources in cosmic ray maps using the Mexican hat wavelet family"

Batista, R. A., Kemp, E., Daniel, B.

An analysis of the sensitivity of gaussian and mexican hat wavelet family filters to the detection of point sources of ultra-high energy cosmic rays was performed. A source embedded in a background was simulated and the number of events and amplitude of this source was varied aiming to check the sensitivity of the method to detect faint sources with low statistic of events.

[P009-12] "Directed and elliptic flow of charged particles in Cu plus Cu collisions at root s(NN)=22.4 GeV"

Agakishiev, G., Aggarwal, M. M., Ahammed, Z., Alakhverdyants, A. V., Alekseev, I., Alford, J., Anderson, B. D., Anson, C. D., et all.

This paper reports results for directed flow v(1) and elliptic flow v(2) of charged particles in Cu + Cu collisions at root s(NN) = 22.4 GeV at the Relativistic Heavy Ion Collider. The measurements are for the 0-60% most central collisions, using charged particles observed in the STAR detector. Our measurements extend to 22.4-GeV Cu + Cu collisions the prior observation that v1 is independent of the system size at 62.4 and 200 GeV and also extend the scaling of v(1) with eta/y(beam) to this system. The measured v(2)(p(T)) in Cu + Cu collisions is similar for root s(NN) throughout the range 22.4 to 200 GeV. We also report a comparison with results from transport model (ultrarelativistic quantum molecular dynamics and multiphase transport model) calculations.The model results do not agree quantitatively with the measured v(1)(eta), v(2)(p(T)), and v(2)(eta).

[P010-12] "Dynamics of atom-field entanglement in a bimodal cavity"

Decordi, G. L., Vidiella-Barranco, A.

In this paper we investigate some aspects of the dynamics and entanglement of bipartite quantum system (atom-quantized field), coupled to a third "external" subsystem (quantized field). We make use of the Raman coupled model; a three-level atom in a lambda configuration interacting with two modes of the quantized cavity field. We consider the far off resonance limit, which allows the derivation of an effective Hamiltonian of a two-level atom coupled to the fields. We also make a comparison with the situation in which one of the modes is treated classically rather than prepared in a quantum field (coherent state).

[P011-12] "Estimations of the distances of stellar collapses in the galaxy by analyzing the energy spectrum of neutrino bursts"

Kemp, E., Miguez, B., Fulgione, W.

The neutrino telescopes of the present generation, depending on their specific features, can reconstruct the neutrino spectra from a galactic burst. Since the optical counterpart could be not available, it is desirable to have at hand alternative methods to estimate the distance of the supernova explosion using only the neutrino data. In this work we present preliminary results on the method we are proposing to estimate the distance from a galactic supernova based only on the spectral shape of the neutrino burst and assumptions on the gravitational binding energy released an a typical supernova explosion due to stellar collapses.

[P012-12] "Estimation of the RBE of mammography-quality beams using a combination of a Monte Carlo code with a B-DNA geometrical model"

Bernal, M. A., de Almeida, C. E., David, M., Pires, E.

The PENELOPE code is used to determine direct strand break yields corresponding to photons from a (60)Co source and 28 and 30 kV x-ray beams impacting on a B-DNA geometrical model, which accounts for five organizational levels of the human genetic material. Direct single, double and total strand break probabilities are determined in a liquid water homogeneous medium with 1.06 g cm(-3) density. The spectra produced by the x-ray beams at various depths in the phantom have been used to study the dependence of the damage yield on the depth. The relative biological effectiveness (RBE) is also estimated using the (60)Co radiation qualities as the reference. According to this work, the damage probabilities and thus the RBE are, within the uncertainties, similar for both x-ray energies and are independent of the depth into the phantom. Furthermore, the total strand break yield is invariant with respect to the energy of the incident photons. The RBE for low-energy x-ray beams determined here (1.3 +/- 0.1) is lower than that reported by Kellerer, taking into account that he used a 200 kV radiation as the reference quality. However, our RBE values are consistent with those determined by Kuhne et al (2005 Radiat. Res. 164 669-76), which used the same biological endpoint and reference quality as our study. Also, our RBE values are similar to those determined by Verhaegen and Reniers (2004 Radiat. Res. 162 592-9).

[P013-12] "Femtoscopy of pp collisions at root s=0.9 and 7 TeV at the LHC with two-pion Bose-Einstein correlations"

Aamodt, K., Quintana, A. A., Adamova, D., Adare, A. M., Aggarwal, M. M., Rinella, G. A., Agocs, A. G., Salazar, S. A., et all.

We report on the high statistics two-pion correlation functions from pp collisions at root s = 0.9 TeV and root s = 7 TeV, measured by the ALICE experiment at the Large Hadron Collider. The correlation functions as well as the extracted source radii scale with event multiplicity and pair momentum. When analyzed in the same multiplicity and pair transverse momentum range, the correlation is similar at the two collision energies. A three-dimensional femtoscopic analysis shows an increase of the emission zone with increasing event multiplicity as well as decreasing homogeneity lengths with increasing transverse momentum. The latter trend gets more pronounced as multiplicity increases. This suggests the development of space-momentum correlations, at least for collisions producing a high multiplicity of particles. We consider these trends in the context of previous femtoscopic studies in high-energy hadron and heavy-ion collisions and discuss possible underlying physics mechanisms. Detailed analysis of the correlation reveals an exponential shape in the outward and longitudinal directions, while the sideward remains a Gaussian. This is interpreted as a result of a significant contribution of strongly decaying resonances to the emission region shape. Significant nonfemtoscopic correlations are observed, and are argued to be the consequence of "mini-jet"-like structures extending to low p(t). They are well reproduced by the Monte-Carlo generators and seen also in pi(+)pi(-) correlations.

[P014-12] "FERM domain interaction with myosin negatively regulates FAK in cardiomyocyte hypertrophy"

Santos, A. M., Schechtman, D., Cardoso, A. C., Clemente, C. F. M. Z., Silva, J. C., Fioramonte, M., Pereira, M. B. M., Marin, T. M., Oliveira, P. S. L., Figueira, A. C. M., Oliveira, S. H. P., Torriani, I. L., Gozzo, F. C., Neto, J. X., Franchini, K. G.

Focal adhesion kinase (FAK) regulates cellular processes that affect several aspects of development and disease. The FAK N-terminal FERM (4.1 protein-ezrin-radixin-moesin homology) domain, a compact clover-leaf structure, binds partner proteins and mediates intramolecular regulatory interactions. Combined chemical cross-linking coupled to MS, small-angle X-ray scattering, computational docking and mutational analyses showed that the FAK FERM domain has a molecular cleft (similar to 998 angstrom(2)) that interacts with sarcomeric myosin, resulting in FAK inhibition. Accordingly, mutations in a unique short amino acid sequence of the FERM myosin cleft, FP-1, impaired the interaction with myosin and enhanced FAK activity in cardiomyocytes. An FP-1 decoy peptide selectively inhibited myosin interaction and increased FAK activity, promoting cardiomyocyte hypertrophy through activation of the AKT-mammalian target of rapamycin pathway. Our findings uncover an inhibitory interaction between the FAK FERM domain and sarcomeric myosin that presents potential opportunities to modulate the cardiac hypertrophic response through changes in FAK activity.

[P015-12] "Glasses-free 3D viewing systems for medical imaging"

Magalhaes, D. S. F., Serra, R. L., Vannucci, A. L., Moreno, A. B., Li, L. M.

In this work we show two different glasses-free 3D viewing systems for medical imaging: a stereoscopic system that employs a vertically dispersive holographic screen (VDHS) and a multi-autostereoscopic system, both used to produce 3D MRI/CT images. We describe how to obtain a VDHS in holographic plates optimized for this application, with field of view of 7 cm to each eye and focal length of 25 cm, showing images done with the system. We also describe a multi-autostereoscopic system, presenting how it can generate 3D medical imaging from viewpoints of a MRI or CT image, showing results of a 3D angioresonance image.

[P016-12] "Heat flow measurements and the order of the magnetic transition in (Dy,Gd)Co(2) solid solutions"

de Sousa, V. S. R., Monteiro, J. C. B., dos Reis, R. D., Medina, A. N., Gama, S., von Ranke, P. J., Gandra, F. C. G.

In this work we present scanning heat flow measurements in the series of compounds Dy(1-x)Gd(x)Co(2) (x = 0, 0.1, 0.2, 0.3) which reveal a first order character in the magnetic transition for x = 0 and 0.1. The isothermal entropy change obtained for a magnetic field variation from 0 to 2T shows good agreement with the calculations based on a model Hamiltonian that takes into account the crystal field, magnetoelastic, exchange and Zeeman interactions. The maximum entropy change varies from 7.0 J/kg K (DyCo(2)) to 1.8 J/kg K (Dy(0.7) Gd(0.3)Co(2)) under a 2T magnetic field variation. The refrigerant cooling power (RCP) varies from 97 J/kg to 67 J/kg across the series. The entropy shows a strong correlation with the transition temperature regardless the transition type.

[P017-12] "Hysteretic giant magnetoimpedance effect analyzed by first-order reversal curves"

Beron, F., Valenzuela, L. A., Knobel, M., Melo, L. G. C., Pirota, K. R.

We applied the first-order reversal curve method to hysteretic giant magnetoimpedance (GMI) of soft magnetic amorphous ribbons with a well-defined transversal domain structure and quasi-anhysteretic magnetization behavior. In opposition to major curve, it gives access to the distribution of local irreversible changes of the transverse permeability, which undergo a gradual transition. Results show that hysteretic GMI effect consists of three distinct regimes depending on the applied field. An interlinked hysteron/anti-hysteron model is proposed to analyze the obtained results, which allows one to follow the influence of frequency and anisotropy upon the irreversible switches probed by GMI.

[P018-12] "Investigation of indirect structural and chemical parameters of GeSi nanoparticles in a silica matrix by combined synchrotron radiation techniques"

Gasperini, A., Malachias, A., Fabbris, G., Kellermann, G., Gobbi, A., Avendano, E., Azevedo, G. D.

The formation of GeSi nanoparticles on an SiO2 matrix is studied here by synchrotron-based techniques. The shape, average diameter and size dispersion were obtained from grazing-incidence small-angle X-ray scattering data. X-ray diffraction measurements were used to obtain crystallite sizes and composition via resonant (anomalous) measurements.

By using these techniques as input for extended X-ray absorption fine structure analysis, the local composition surrounding the Ge atoms is investigated. Although the results for each of the methods above are commonly analyzed separately, the combination of such techniques leads to an improved understanding of nanoparticle structural and chemical properties. Crucial indirect parameters that cannot be quantified by other means are accessed in this work, such as local strain, the possibility of forming coreshell structures, the fraction of Ge atoms diluted in the matrix (not forming nanoparticles), the amorphous and crystalline Ge fractions, and the relative population of nanoparticles with single and multiple crystalline domains.

[P019-12] "Longitudinal dependence of two-particle momentum correlations from the hydrodynamic flow model NEXSPHERIO"

Sharma, M., Pruneau, C., Gavin, S., Takahashi, J., de Souza, R. D., Kodama, T.

The rapidity dependence of two-particle momentum correlations can be used to probe the viscosity of the liquid produced in heavy nuclei collisions at the Relativistic Heavy Ion Collider (RHIC). We reexamine this probe in light of the recent experimental analyses of the azimuthal-angle dependence of number correlations, which demonstrate the importance of initial state fluctuations propagated by hydrodynamic flow in these correlations. The NEXSPHERIO model combines fluctuating initial conditions with viscosity-free hydrodynamic evolution and, indeed, has been shown to describe azimuthal correlations. We use this model to compute the number density correlation R(2) and the momentum current correlation function C, at low transverse momentum in Au + Au collisions at root s(NN) = 200 GeV. The correlation function C is sensitive to details of the collision dynamics. Its longitudinal width is expected to broaden under the influence of viscous effects and narrow in the presence of sizable radial flow. While the NEXSPHERIO model qualitatively describes the emergence of a near-side ridge-like structure for both the R(2) and C observables, we find that it predicts a longitudinal narrowing of the near-side peak of these correlation functions for increasing number of participants in contrast with recent observations by the STAR Collaboration of a significant broadening in most central collisions relative to peripheral collisions.

[P020-12] "Magnetic and Dielectric Proprieties of Multiferroic (1-x)Pb(Fe2/3W1/3)O-3-xPbTiO(3) Ceramics Prepared Via a Modified Two-stage Solid-state Reaction"

Fraygola, B. M., Coelho, A. D., Garcia, D., Eiras, J. A.

Multiferroic $Pb(Fe2/3W1/3)O-3-PbTiO3$ (PFW-PT) ceramics were synthesized via a modified two-stage solid-state reaction. This method utilized $Fe2WO6$, prepared at a first-stage, which was subsequently reacted with a stoichiometric amount of PbO and $TiO2$ at the second stage. This procedure efficiently suppressed the formation of lead tungstates and leads to getting dense ceramics. Electric and dielectric properties of $(1-x)Pb(Fe2/3W1/3)O-3-xPbTiO(3)$ solid solutions were investigated as a function of the frequency and temperature. All samples present density higher than 96% of the theoretical one, low percentage of pyrochlore phase (<2%) and relatively high electrical resistivity ($<10(10)$ Omega.m). RF dielectric measurements over the temperature showed the presence of a peak, which is related to the ferro-paraelectric phase transition and conductive contributions (in the range 200-700K), associated to a electronic hoping mechanism. The dielectric properties of the PFW shows a typical relaxor behaviour for

x = 0 and 0.10 with frequency-dependent peak temperature (Tm), while the samples with higher PT-content undergo a 'normal' para-ferroelectric transition at the Curie temperature T-c. The FE phase transition of PFW is shifted to higher temperatures by $PbTiO3$ (PT) additions and high resistivity are obtained for PT containing samples. Different types of magnetic activity dependent on composition and temperature were found.

[P021-12] "Magnetic ordering and instability investigation of multiferroic Pb(Fe(2/3)W(1/3))O(3) ceramics by microwave dielectric spectroscopy"

Fraygola, B., Coelho, A. A., Garcia, D., Eiras, J. A.

The microwave dielectric and magnetic properties of $Pb(Fe(2/3)W(1/3))O(3)$ multiferroic ceramics were investigated. A dielectric dispersion occurring in the frequency range 100 MHz-3 GHz and in a broad temperature range showed itself to be a powerful tool to detect magnetostrictive effects. The experimental results revealed the following remarkable features: the temperature dependence of f(R) (characteristic frequency) and the dielectric strength Delta epsilon (characteristic of the dispersion) enabled us to identify not only the para-ferroelectric (T(C) approximate to 180 K) but also the para-antiferromagnetic (T(N) approximate to 340 K) phase transitions, while magnetic measurements revealed the para-antiferromagnetic ordering and a weak superexchange interaction (T(N2) similar to 15 K). Additionally, both characterizations confirmed the existence of structural or magnetic instabilities around 250 K.

[P022-12] "Monte Carlo simulation of energy-deposit clustering for ions of the same LET in liquid water"

Francis, Z., Incerti, S., Ivanchenko, V., Champion, C., Karamitros, M., Bernal, M. A., El Bitar, Z.

This work presents a Monte Carlo study of energy depositions due to protons, alpha particles and carbon ions of the same linear-energy-transfer (LET) in liquid water. The corresponding track structures were generated using the Geant4-DNA toolkit, and the energy deposition spatial distributions were analyzed using an adapted version of the DBSCAN clustering algorithm. Combining the Geant4 simulations and the clustering algorithm it was possible to compare the quality of the different radiation types. The ratios of clustered and single energy depositions are shown versus particle LET and frequency-mean lineal energies. The estimated effect of these types of radiation on biological tissues is then discussed by comparing the results obtained for different particles with the same LET.

[P023-12] "MRI-Texture Analysis of Corpus Callosum, Thalamus, Putamen, and Caudate in Machado-Joseph Disease"

de Oliveira, M. S., D'Abreu, A., Franca, M. C., Lopes-Cendes, I., Cendes, F., Castellano, G.

BACKGROUND/PURPOSE - Texture analysis (TA) is a branch of image processing, which attempts to convey "texture" information from digital images, such as magnetic resonance images (MRI). Machado-Joseph disease (MJD) affects mainly

cerebellum and brainstem, but recent studies have shown that other cerebral structures may also be affected.

OBJECTIVE - To investigate subtle structural abnormalities in corpus callosum (CC), thalami, putamen, and caudate nuclei of patients with MJD using TA.

METHODS Eighteen healthy volunteers and 18 patients with MJD were studied (mean age at disease onset = 34.7 years; disease duration = 9.6 years; mean expanded CAG in the MJD1 gene = 73). A TA approach based on the gray-level cooccurrence matrix was applied to T1-MRI. Regions of interest were manually segmented for each subject, and texture parameters were computed for each of the aforementioned anatomical structures.

RESULTS - TA parameters showed differences between the 2 groups for the caudate nuclei, thalami, and putamen. No differences were found for the CC.

CONCLUSIONS - TA was capable of detecting tissue alterations in MRI of patients with MJD. These alterations were in areas already shown to be affected by histopathological studies. In addition, we confirmed the thalamic involvement in patients with MJD, which had only been demonstrated in volumetric studies.

[P024-12] "Positron scattering from methane"

Zecca, A., Chiari, L., Trainotti, E., Sarkar, A., Sanchez, S. D., Bettega, M. H. F., Varella, M. T. N., Lima, M. A. P., Brunger, M. J.

We report on measurements of total cross sections for positron scattering from the fundamental organic molecule methane (CH(4)). The energy range of these measurements was 0.1-50 eV, whereas the energy resolution was similar to 100 meV when our Ni moderator was used and similar to 260 meV when the W moderator was employed. To assist us in interpreting these data, Schwinger multichannel calculations were performed at both static and static plus polarization levels of approximation for elastic positron scattering from 0.001 to 10 eV. These calculations are found to be in quite good qualitative agreement with our measured data, and they clearly educe the crucial role played by the target polarization in the low energy positron-CH(4) scattering dynamics.

[P025-12] "Pressure effects on the transitions between disordered phases in supercooled liquid silicon"

Garcez, K. M. S., Antonelli, A.

We investigate the pressure effects on the transitions between the disordered phases in supercooled liquid silicon through Monte Carlo simulations and efficient methods to compute free energies. Our calculations, using an environment dependent interatomic potential for Si, indicate that at zero pressure the liquid-liquid phase transition, between the high density liquid and the low density liquid, occurs at a temperature 325K below melting. We found that the liquid-liquid transition temperature decreases with increasing pressure, following the liquid-solid coexistence curve. As pressure increases, the liquid-liquid coexistence curve approaches the region where the glass transition between the low density liquid and the low density amorphous takes place. Above 5 GPa, our calculations show that the liquid-liquid transition is suppressed by the glassy dynamics of the system. We also found that above 5 GPa, the glass transition temperature is lower than that at lower pressures, suggesting that under these conditions the glass transition occurs between the high density liquid and the high density amorphous.

[P026-12] "Recent Results from the Pierre Auger Observatory"

Dobeigkeit, C.

The Pierre Auger Observatory in Argentina is the largest cosmic ray detector array ever built. Its main goal is to measure cosmic rays of energy above 10(18) eV with unprecedented statistics and precision. Although the construction of its baseline design was completed in mid-2008, the Observatory has been taking data continuously since January 2004. The main results obtained with the Pierre Auger Observatory are presented, with emphasis on the energy spectrum and studies of composition and arrival directions of the ultrahigh energy cosmic rays. Features observed in the energy spectrum are discussed. Results about cosmic ray composition inferred from systematic studies of the average depth of shower maximum and its fluctuations are reviewed. Recent results of studies of arrival direction distributions and correlations with. nearby extragalactic objects are presented.

[P027-12] "Ronchi-grating-based measurement of photorefractive recording response time"

de Oliveira, I., Frejlich, J.

We report on a simple technique for the measurement of the recording response time in photorefractive materials. Three different material samples were successfully measured, and their response times, as well as their dependence upon the recording/measurement light irradiance, were also determined and compared with available data in the literature in order to assess the reliability of this technique.

[P028-12] "Search for ultrahigh energy neutrinos in highly inclined events at the Pierre Auger Observatory"

Abreu, P., Aglietta, M., Ahn, E. J., Albuquerque, I. F. M., Allard, D., Allekotte, I., Allen, J., Allison, P., Castillo, J. A., Alvarez-Muniz, J., Ambrosio, M., Aminaei, A., Anchordoqui, L.

The Surface Detector of the Pierre Auger Observatory is sensitive to neutrinos of all flavors above 0.1 EeV. These interact through charged and neutral currents in the atmosphere giving rise to extensive air showers. When interacting deeply in the atmosphere at nearly horizontal incidence, neutrinos can be distinguished from regular hadronic cosmic rays by the broad time structure of their shower signals in the water-Cherenkov detectors. In this paper we present for the first time an analysis based on down-going neutrinos. We describe the search procedure, the possible sources of background, the method to compute the exposure and the associated systematic uncertainties. No candidate neutrinos have been found in data collected from 1 January 2004 to 31 May 2010. Assuming an E(-2) differential energy spectrum the limit on the single-flavor neutrino is E(2)dN/dE < 1.74 x 10(-7)GeVcm(-2)s(-1)sr(-1) at 90% C.L. in the energy range 1 x 10(17) eV < E < 1 x 10(20)eV.

[P029-12] "Spin injection from two-dimensional electron and hole gases in resonant tunneling diodes"

Gobato, Y. G., Galeti, H. V. A., dos Santos, L. F., Lopez-Richard, V., Cesar, D. F., Marques, G. E., Brasil, M. J. S. P., Orlita, M., Kunc, J., Maude, D. K., Henini, M., Airey, R. J.

We have investigated the polarized-resolved photoluminescence from the contact layers and the quantum-well in an n-type GaAs/GaAlAs resonant tunneling diode for magnetic fields up to 19 T. The optical emission from the GaAs contact layers comprises the recombination from highly spin-polarized two-dimensional electron and hole gases with free tunneling carriers. Both the energy position and intensity of this indirect recombination are voltage-dependent and show remarkably abrupt variations near scattering-assisted tunneling resonances. Our results show that these two dimensional gases act as spin-polarized sources for carriers tunneling through the well in resonant tunneling diodes.

[P030-12] "Structure and energetics of extended defects in ice I-h"

Silva, D. L., de Koning, M.

We consider the molecular structure and energetics of extended defects in proton-disordered hexagonal ice I-h. Using plane-wave density functional theory (DFT) calculations, we compute the energetics of stacking faults and determine the structure of the 30 degrees and 90 degrees partial dislocations on the basal plane. Consistent with experimental data, the formation energies of all fully reconstructed stacking faults are found to be very low. This is consistent with the idea that basal-plane glide dislocations in ice I-h are dissociated into partial dislocations separated by an area of stacking fault. For both types of partial dislocation we find a strong tendency toward core reconstruction through pairwise hydrogen-bond reformation. In the case of the 30 degrees dislocation, the pairwise hydrogen-bond formation leads to a period-doubling core structure equivalent to that seen in zinc-blende semiconductor crystals. For the 90 degrees partial we consider two possible core reconstructions, one in which the periodicity of the structure along the core remains unaltered and another in which it is doubled. The latter is preferred, although the energy difference between both is rather small, so that a coexistence of both reconstructions appears plausible. Our results imply that a mobility theory for dislocations on the basal plane in ice I-h should be based on the idea of reconstructed partial dislocations.

[P031-12] "Sub-THz and H alpha activity during the preflare and main phases of a goes class M2 event"

Kaufmann, P., Marcon, R., de Castro, C. G. G., White, S. M., Raulin, J. P., Correia, E., Fernandes, L. O., de Souza, R. V., Godoy, R., Marun, A., Pereyra, P.

Radio and optical observations of the evolution of flare-associated phenomena have shown an initial and rapid burst at 0.4 THz only followed subsequently by a localized chromospheric heating producing an Ha brightening with later heating of the whole active region. A major instability occurred several minutes later producing one impulsive burst at microwaves only, associated with an M2.0 GOES X-ray flare that exhibited the main Ha brightening at the same site as the first flash. The possible association between long-enduring time profiles at soft X-rays, microwaves, Ha, and sub-THz wavelengths is discussed. In the decay phase, the Ha movie shows a disrupting magnetic arch structure ejecting dark, presumably chromospheric, material upward. The time sequence of events suggests genuine interdependent and possibly non-thermal instabilities triggering phenomena, with concurrent active region plasma heating and material ejection.

[P032-12] "System size and energy dependence of near-side dihadron correlations"

Agakishiev, G., Aggarwal, M. M., Ahammed, Z., Alakhverdyants, A. V., Alekseev, I., Alford, J., Anderson, B. D., Anson, C. D., Arkhipkin, D., et all.

Two-particle azimuthal (Delta phi) and pseudorapidity (Delta eta) correlations using a trigger particle with large transverse momentum (p(T)) in d+Au, Cu+Cu, and Au+Au collisions at root s(NN) = 62.4 GeV and 200 GeV from the STAR experiment at the Relativistic Heavy Ion Collider are presented. The near-side correlation is separated into a jet-like component, narrow in both Delta phi and Delta eta, and the ridge, narrow in Delta phi but broad in Delta eta. Both components are studied as a function of collision centrality, and the jet-like correlation is studied as a function of the trigger and associated p(T). The behavior of the jet-like component is remarkably consistent for different collision systems, suggesting it is produced by fragmentation. The width of the jet-like correlation is found to increase with the system size. The ridge, previously observed in Au+Au collisions at root s(NN) = 200 GeV, is also found in Cu+Cu collisions and in collisions at root s(NN) = 62.4 GeV, but is found to be substantially smaller at root s(NN) = 62.4 GeV than at root s(NN) = 200 GeV for the same average number of participants (< N(part)>). Measurements of the ridge are compared to models.

[P033-12] "The effect of the geomagnetic field on cosmic ray energy estimates and large scale anisotropy searches on data from the Pierre Auger Observatory"

Abreu, P., Aglietta, M., Ahn, E. J., Albuquerque, L. F. M., Allard, D., Allekotte, I., Allen, J., et all.

We present a comprehensive study of the influence of the geomagnetic field on the energy estimation of extensive air showers with a zenith angle smaller than 60 degrees, detected at the Pierre Auger Observatory. the geomagnetic field induces an azimuthal modulation of the estimated energy of cosmic rays up to the similar to 2% level at large zenith angles. We present a method to account for this modulation of the reconstructed energy. We analyse the effect of the modulation on large scale anisotropy searches in the arrival direction distributions of cosmic rays. At a given energy, the geomagnetic effect is shown to induce a pseudo-dipolar pattern at the percent level in the declination distribution that needs to be accounted for.

[P034-12] "The ethanol electrooxidation at Pt layers deposited on polycrystalline Au"

Prieto, M. J., Rodrigues, U. P., Landers, R., Tremiliosi, G.

The ethanol electro-oxidation reaction was evaluated using a polycrystalline Au substrate modified with two different amounts of Pt using the galvanic exchange methodology. FTIR results suggest that Pt deposits have a greater ability to break the C-C bond present in the ethanol molecule. However, under potentiostatic conditions both modified Au surfaces undergo faster deactivation in comparison with polycrystalline platinum as indicated by the chronoamperometric results. XPS results indicate the presence of two phases depending on the Pt content. These are: (i) Pt-Au alloy and (ii) segregated Pt. The structural and electronic properties of these phases were related to the differences observed in the catalytic activity.

[P035-12] "The Lateral Trigger Probability function for the Ultra-High Energy Cosmic Ray showers detected by the Pierre Auger Observatory"

Abreu, P., Aglietta, M., Ahn, E. J., Albuquerque, I. F. M., Allard, D., Allekotte, I., Allen, J., Allison, P., Castillo, J. A., Alvarez-Muniz, J., Ambrosio, M., et all.

In this paper we introduce the concept of Lateral Trigger Probability (LTP) function, i.e., the probability for an Extensive Air Shower (EAS) to trigger an individual detector of a ground based array as a function of distance to the shower axis, taking into account energy, mass and direction of the primary cosmic ray. We apply this concept to the surface array of the Pierre Auger Observatory consisting of a 1.5 km spaced grid of about 1600 water Cherenkov stations. Using Monte Carlo simulations of ultra-high energy showers the LTP functions are derived for energies in the range between 10(17) and 10(19) eV and zenith angles up to 65 degrees. A parametrization combining a step function with an exponential is found to reproduce them very well in the considered range of energies and zenith angles. The LTP functions can also be obtained from data.

[P036-12] "Theoretical investigation on electron scattering by benzene in the intermediate-energy range"

de Souza, G. L. C., dos Santos, A. S., Lucchese, R. R., Machado, L. E., Brescansin, L. M., Manini, H. V. Iga, I., Lee, M. T.

We present a theoretical investigation on electron scattering by benzene (C_6H_6) in the intermediate-energy range. Calculated elastic differential, integral, and momentum-transfer as well as total (elastic + inelastic) and total absorption cross sections are reported for impact energies ranging from 20 to 500 eV. A complex optical potential is used to represent the electron-molecule interaction dynamics. A theoretical method based on the single-center-expansion close-coupling framework and corrected by the Pade approximant [F. A. Gianturco, R. R. Lucchese, N. Sanna, J. Chem. Phys. 102 (1995) 5743] is used to solve the scattering equations. The comparison of our calculated results with the experimental and theoretical data available in the literature is encouraging.

[P037-12] "Vanadium oxide intercalated with polyelectrolytes: Novel layered hybrids with anion exchange properties"

Quites, F. J., Bisio, C., Vinhas, R. D. G., Landers, R., Marchese, L., Pastore, H. O.

Novel anion exchange hybrid materials were developed by the insertion of poly(diallymethylammonium chloride) (PDDACl) and poly(allylamine hydrochloride) (PAHCl) polyelectrolytes into V2O5 interlayer spaces using hydrothermal treatment and were used to host an anionic cyanine dye. A systematic study of the hybrid material synthesis by direct in situ reaction of PDDACl and PAHCl polycations with V2O5 powders showed that the interlayer space of V2O5 expands from 0.44 nm to 1.40 nm and 1.80 nm upon intercalation of PDDACl and PAHCl polyelectrolytes, respectively. X-ray photoelectron spectroscopy and DR UV-Vis-NIR spectroscopy revealed that some V' sites were reduced to V' during the intercalation of the polyelectrolytes, these acted as both charge balancing entities for the negative oxide sheets and carriers for exchange sites located in the V2O5 interlayer space. The interlayer separation is consistent with the existence of coiled conformation of the polycations. The hybrid materials produced [PDDACl](0.24)[PDDA](0.29)V2O5 and [PAHCl](0.28)[PAH](0.47)V2O5, exhibited approximately 45.0% and 37.0% of chloride ions still available for anionic exchange, respectively. These materials were used to encapsulate a cyanine anionic dye. The presence of the dye was evidenced in the [PDDACL](0.24)[PDDA](0.29)V2O5 by significant fluorescence, with emission peak centered at 617 nm.

[P038-12] "Zeeman splitting and spin dynamics tuning by exciton charging in two-dimensional systems"

Castelano, L. K., Cesar, D. F., Lopez-Richard, V., Marques, G. E., Couto, O. D. D., Iikawa, F., Hey, R., Santos, P. V.

We report a study of magnetic responses of neutral and charged excitons in quantum wells, which are very sensitive to the strong spin hybridization of holes. This effect can be used to engineer the spin character of excitonic complexes in two-dimensional systems tuned by the magnetic field strength. Conditions for spin flip for each kind of excitonic complex is detailed and the nature of the effect discussed. Differences in the effective Zeeman splitting between neutral and charged excitons are theoretically predicted and unambiguously confirmed experimentally. Circularly polarized resolved photoluminescence has been used to study these effects under applied magnetic fields. The intertwining of spin dynamics of excitons and trions is discussed.

Material Editorial

"Comment on 'Quantum Thermal Bath for Molecular Dynamics Simulation'"
Barrozo, A. H., de Koning, M.

Abstracta